Towards low cost grid scale energy storage: supercapacitors based on up-cycled industrial mill scale waste

Chaopeng Fu,* Patrick S. Grant

Department of Materials, University of Oxford, Oxford, United Kingdom, OX1 3PH.

* E-mail: chaopeng.fu@materials.ox.ac.uk

Abstract

Mill scale is a waste product from the steel industry available cheaply in tonne quantities and consisting of various iron oxides. The supercapacitive behaviour of mill scale directly from the steel plant, and after various cheap and scalable physical and chemical treatments, has been studied in electrodes formed by spraying mill-scale containing suspensions onto large area current collectors. Half-cell and full cell supercapacitors in cheap, non-toxic aqueous sodium sulphite electrolyte were investigated by cyclic voltammetry, charge-discharge and electrochemical impedance spectroscopy, and delivered a capacitance of up to 92 F g^{-1} at a scan rate of 5 mV s^{-1}, which was maintained at more than 80% after 5,000 cycles. The approximate costs of commercial and mill scale-based supercapacitors were compared, and showed that while mill scale absolute capacitances were lower than more expensive laboratory synthesised metal oxides, the cost per kilo-watt performance can be competitive, especially for very large grid scale storage applications.

Keywords: supercapacitor, mill scale, iron oxides, low cost, waste

Introduction

Supercapacitors, also called electrochemical capacitors, have comparatively high power density and long cycle life and are of interest to replace or complement more energy dense lithium-ion and other batteries in transport and stand-alone or grid-connected power plants, as well as portable electronics. There are two principal types of supercapacitor electrode materials: high surface area, usually carbon-based materials that facilitate adsorption/desorption of electrolyte ions at the electrode/electrolyte interface to form an electrical double layer with specific capacitance usually in the range 80-200 F g^{-1};[1-3] and transition metal oxides or conducting polymers that store electrical charge through fast and reversible redox reactions at their surfaces, usually termed pseudo-capacitors and with specific capacitance that might exceed 200 F g^{-1}.[4, 5] Although carbonaceous electrodes dominate commercial applications, there are intense research efforts focused on transition metal oxides because of the potential increases in energy density they might afford, if their disadvantages of restricted power density, poor cycle life and usually high cost might be mitigated.[6-8]

The most studied pseudo-capacitive materials are ruthenium oxide[9, 10] and manganese oxide,[11-14] and both have achieved commercial impact in niche markets. Recently, there have been sustained efforts to develop other metal oxides such as those of nickel oxide and cobalt oxide to similar levels of maturity and scale.[15-18] However, despite attractive laboratory performance in these latter systems, many of the transition metal oxide-based system have so far remained either inherently expensive and/or involve complex synthesis that places restriction on their scalability. Therefore there is a continuing opportunity to develop systems that realise some of

the potential of transition metal oxides, particularly in energy density, while using low-cost and environmentally benign materials combined with scalable processing routes. Many of these considerations, particularly relating to cost, safety and scalability, become more acute when large grid-scale energy storage systems are considered.

Iron oxides have also been considered as supercapacitor electrodes since they exhibit some advantageous characteristics, such as natural abundance, low-cost, low-toxicity and environmental friendliness.[19-23] For example, Fe_2O_3 nanostructures prepared via an electrospinning technique using ferric acetyl acetonate and heat treatment at 500 °C showed a capacitance of up to 256 F g^{-1} at a slow scan rate of 1 mV s^{-1} in 1 M LiOH electrolyte.[19] Porous flower-like Fe_2O_3 nanostructures by an ethylene glycol mediated self-assembly process delivered a capacitance of 127 F g^{-1} at 1 A g^{-1} in 0.5 M Na_2SO_3.[22] Fe_3O_4 has also been studied and in a nanowire format delivered > 100 F g^{-1} at 250 mV s^{-1} in a Na_2SO_3 electrolyte.[24, 25] Although possessing high performance, these “in-house” materials are available so far only at the laboratory scale and few could be scaled practicably to industrial application.

For carbon-based electric double layer capacitor electrodes, researchers have sought to reduce costs for large scale deployments by using bio-derived sources of carbon, such as cellulose of different types, bananas, coconuts, peanuts, used cigarette filters, etc.[26-28] However, to the best of our knowledge, there have been no similar efforts to investigate cheap or waste materials for pseudo-capacitors. In this paper we investigate the possibility of up-cycling mill scale to an energy storage material, which is a super-abundant waste product that is created as a by-

product of many metallurgical processes in the steel industry and is cheaply available in tonne quantities. Iron-based oxide layers are readily formed on the surface of commonly used steel billets and sheets during processing, and are then cracked and dispersed each time the steel undergoes one of many hot-rolling passes, so that many tonnes of mill scale soon accumulate within a large integrated steel plant. The mill scale is primarily a mix of iron oxides, which we combine with a scalable spray processing technique to fabricate supercapacitor electrodes for possible grid scale storage applications. While no claims are made that the resulting energy storage performance, e.g. Farads per unit weight, is competitive with laboratory synthesised iron oxides, we then use cost estimations to show that the mill scale's cost-weighted storage behaviour may be competitive with current technologies, and suggest ways in which this performance might be improved further. We also advocate the development of standard approaches to cost-performance assessments that will allow more robust cross-comparisons between emerging energy storage materials systems, especially for grid applications.

Experimental

Processing of mill scale electrodes

Mill scale as shown in Fig. 1 was supplied directly from a rolled steel plant by Tata Steel Long Products, UK. The multi-kg mill scale chunks were pulverized firstly by planetary ball mill (Fritsch Pulverisette 5) using a stainless steel milling bowl and balls in ethanol at a material-to-ball weight ratio of 1:10. Ball milling was then performed at 300 rpm for times of 4 to 12 hr. After ball milling, the refined mill scale powders were chemically treated in 0.1 M HCl solution under ultrasound, and then washed and dried overnight at 80 °C under vacuum. Electrodes

were formed by spray deposition of mill scale suspensions, which is described in detail elsewhere.[29] Briefly, the mill scale powder and carbon black to facilitate electron transfer with a mass ratio of 90:10 were suspended in a 1:1 water: ethanol mixture. The suspension was sonicated for 15 minutes (Sonics and Materials Vibra Cell VC750) and the well-dispersed suspension immediately sprayed at an atomising air pressure of 1 bar onto large area stainless steel (SS) sheets and/or Al foils held flat on a vacuum chuck hotplate maintained at a temperature of 90 ^{o}C. The spray was reciprocated over the substrate in a zig-zag pattern at a stand-off distance of 10 cm to produce an electrode with a thickness of ~30 μm.

Material and electrode characterization

Scanning electron microscopy (SEM) images of the mill scale at each stage of processing were obtained in a JEOL JSM-6500F, and X-ray diffraction of powder samples was conducted in a Siemens D5000 powder diffractometer with Cu Kα and a 2θ step size of 0.05°. X-ray photoelectron spectroscopy spectra were obtained in a K-Alpha Fisher scientific system with Al X-ray source. Electrode thickness was determined by a series of step height measurements using a profilometer (Dektak 6M Veeco Instruments Inc.). The Brunauer-Emmett-Teller (BET) surface area of the mill scale in different conditions was measured using N_2 adsorption/desorption behaviour (Micrometrics Gemini VI). The mass of spray deposited material was measured by weighing of the substrates before and after spraying using a microbalance with 0.01 mg readability (Sartorius).

Electrochemical measurements

Electrochemical testing of the electrodes was conducted in a three-electrode cell using a Pt sheet counter electrode, a Ag/AgCl reference electrode and a Gamry ref 600 potentiostat in 0.5M Na_2SO_3 solution at room temperature. Na_2SO_3 was chosen because as well as surface redox reactions with iron oxides it also provides additional reversible redox reaction of the sulphite ions.[23] Cyclic voltammetry was performed in a potential range from -0.05 to -1.05 V vs Ag/AgCl at scan rates from 5 to 200 mV s^{-1}. Galvanostatic charge/discharge tests were performed at current densities of 0.5-3 A g^{-1}. Electrochemical impedance spectroscopy (EIS) was performed in the frequency range of 100 KHz to 0.01 Hz at open circuit potential with an amplitude of 5 mV. Symmetric, full cell supercapacitors using two identical mill scale sprayed electrodes with a glass fibre separator were also fabricated and investigated in a 2032 coin cell configuration using similar techniques.

Results and discussion

A schematic diagram showing the processing route of the mill scale is presented in Fig. 1. The as-received mill scale chunks were pulverised to powder. As the ball milling time increased from 4 to 12 hr the SEM images in Fig. 2 suggested that the particles reduced in size, while maintaining a flattened, angular shape that made quantified measurement of diameter, for example by laser diffraction, unreliable. After 4 hr, the particle dimensions were in the range 1 to 10 μm, and sizes reduced further after 12 hr to the range 50 nm to 5 μm with most particles having dimensions of ~ 1 μm. When the ball milling time exceeded 12 hr, the powder size did not change noticeably, and 12 hr was considered the maximum useful milling time. The mill scale powder was then etched in a dilute HCl solution, as shown in Fig. 2d. Compared with un-

etched powder in Fig. 2c, the surface morphology showed a more porous surface of etched "pits". The yield, defined as mass percentage of useful powder for electrode formation as a proportion of the mill scale chunks was ~80%.

The surface area of the powders at different stages of processing was estimated by N_2 adsorption-desorption and application of the BET method to the resulting isotherms, which are shown in Fig. S1 while Table 1 lists the BET surface areas. The surface area increased slightly with increasing ball milling time, and again on chemically etching, but overall the surface areas were generally lower than conventionally desired for effective pseudo-capacitor materials, and this points to strategies for subsequent improvements.

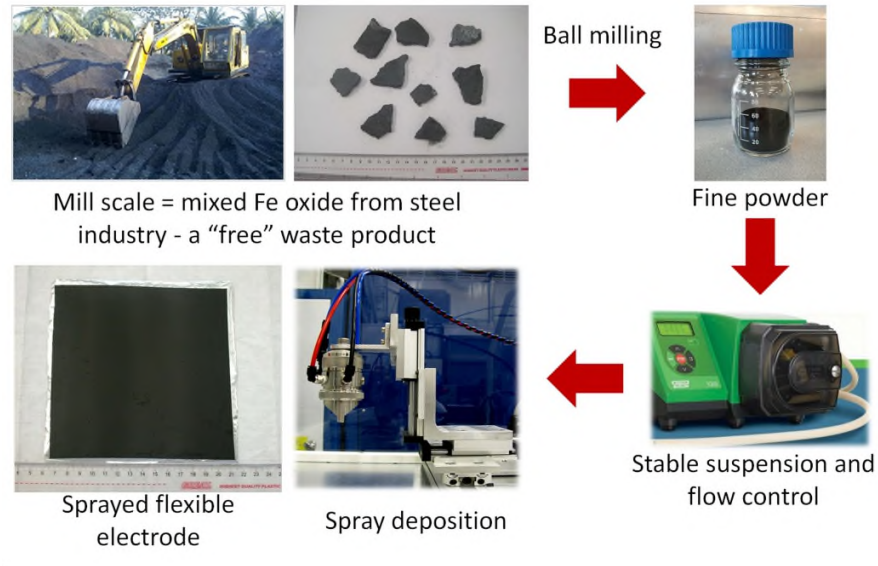

Figure 1 Schematic diagram of the various processing stages to convert mill scale waste from the steel plant to sprayed, large area, 30 µm thick FeO_x based supercapacitor electrodes.

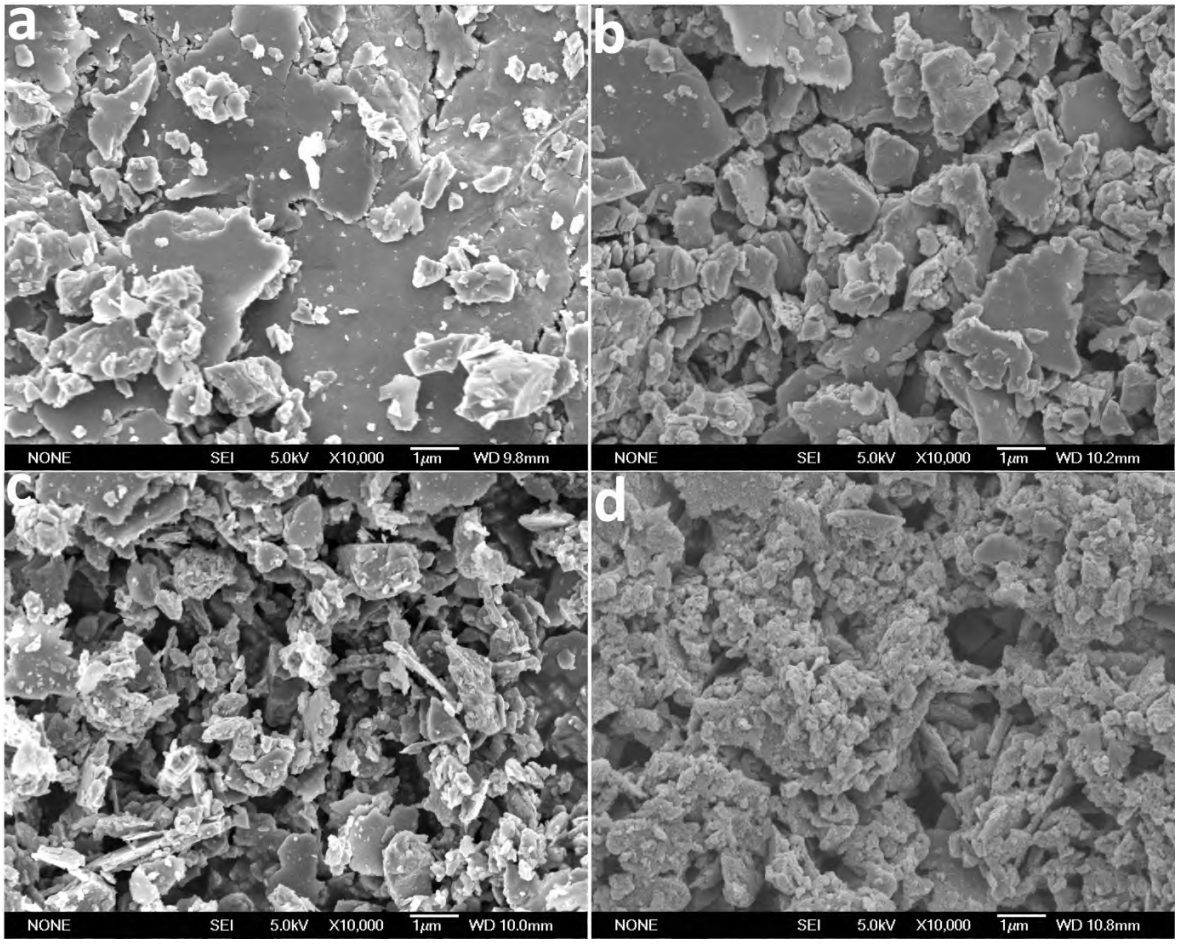

Figure 2 SEM images of the mill scale processed by ball milling for (a) 4 hr, (b) 8 hr, (c) 12 hr, and (d) after chemical etching in HCl

Table 1 BET surface area of the mill scale at different stages of processing

Milling time	**4 hr**	**8 hr**	**12 hr**	**Chemical etching in HCl**
BET surface area (m^2g^{-1})	4.0	5.7	8.4	9.5
Standard error	0.15	0.05	0.16	0.14

Fig. 3 shows the X-ray diffraction trace for the HCl etched mill scale powder, where each of the significant diffraction peaks were ascribed to the various iron oxides Fe_2O_3, Fe_3O_4 and $Fe_{0.942}O$,

and a weak diffraction response from body centred cubic iron. The fraction of each phase was estimated by matching the peak intensities to the corresponding International Centre for Diffraction Data powder patterns, while assuming all phases present were crystalline and there was no preferred orientation.[30-32] The weight fraction of each phase was estimated using a modified internal standard method that takes the I/I_C ratio where I is the intensity of the main peak for the particular phase in question and I_C is the intensity of the strongest peak from α-Al_2O_3 powder mixed into the sample in a 1:1 by weight mixture.[31, 33] As a result, the fraction of Fe_2O_3, Fe_3O_4, $Fe_{0.942}O$, and Fe in the mill scale was estimated by weight as 10%, 40%, 30% and 20% respectively. Additionally, XPS was performed to trace any possible contamination, and no detectable impurity was recognized shown in Fig. S2.

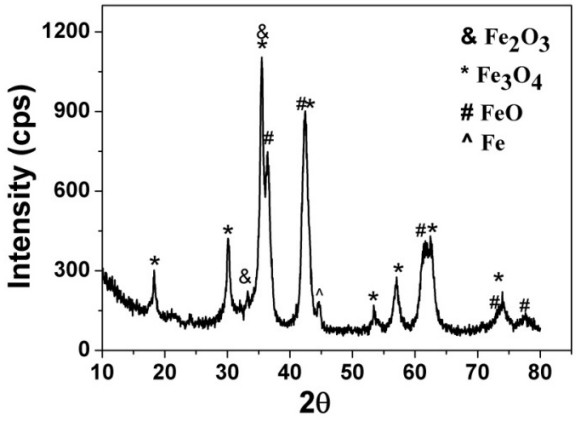

Figure 3 XRD pattern of the ball milled and then HCl etched mill scale.

As shown in Fig. 1, the mill scale fine powders were then suspended in the fugitive water-ethanol carrier and spray deposited onto large area current collectors to a thickness of ~30 μm as shown in Fig. S3. Fig. 4a shows the cyclic voltammetry (CV) curves of electrodes from the mill scale ball milled for 4, 8 and 12 hr, and then HCl etched, each at a potential scan rate of 25 mV

s^{-1}. Overall, the current density increased with increasing ball milling time and on etching, with the etched mill scale displaying the largest current density because of its larger surface area. All subsequent data focuses on powders after 12 hr milling and acid etching only, which is denoted as FeO_x for convenience.

CV curves of the FeO_x electrodes at scan rates from 5 to 200 mV s^{-1} in 0.5 M Na_2SO_3 solution are shown in Fig. 4b, and no significant changes were remarked in the CV shape during CV scans. As expected, there were pseudo-capacitive peaks superimposed on an underlying, distorted rectangular shape typical of the low electrical conductivity of oxide based electrodes. There were two pairs of wide redox peaks due to Fe^{3+} and Fe^{2+} species and the redox reactions associated with adsorbed SO_3^{2-} ions:[25, 34]

$$Fe^{3+} + e^- \leftrightarrow Fe^{2+} \quad (1)$$

$$2SO_3^{2-} + 3H_2O + 4e^- \leftrightarrow S_2O_3^{2-} + 6OH^- \quad (2)$$

$$S_2O_3^{2-} + 3H_2O + 8e^- \leftrightarrow 2S^{2-} + 6OH^- \quad (3)$$

Post cycling XRD showed loss of resolution of peaks due to $Fe_{0.942}O$, reflecting its comparative instability. All the CV curves displayed a similar shape, maintaining the quasi-rectangular shape from 5 mV s^{-1} to 200 mV s^{-1}, suggesting reasonable charge transfer and rate performance. Specific capacitance *C* based on the total mass of electrode materials was calculated from the CV curves according to:[35, 36]

$$C = \frac{\int IdE}{vmE} \quad (4)$$

where *I* is the current, *v* is the scan rate, *m* is the total electrode mass (mill scale plus carbon black), and *E* is the potential range. The specific capacitance (normalized to total electrode

mass) at different scan rate is shown in Fig. 5a, with a specific capacitance of 92 F g^{-1} at 5 mV s^{-1}, reducing with increasing scan rate to 37 F g^{-1} at 200 mV s^{-1}. The capacitance decrease with scan rate was comparatively slow for an iron oxide based supercapacitor, probably because the small fraction metallic Fe helped to prolong electron mobility at higher rates before more strongly resistive behaviour began to dominate.

Galvanostatic charge/discharge tests at different current densities are shown in Fig. 5b. As expected for a transition metal oxide, the charge/discharge curves displayed a slight deviation from the linear response of electric double layer capacitance only, and were typical of iron oxides.[21, 23, 25] Average specific capacitance *C* based on the total mass of electrode materials was also calculated from these discharge curves according to:[23]

$$C = \frac{I}{\frac{dV}{dt}m} \qquad (5)$$

where d*V*/d*t* is the slope of discharge curve, *m* is the total mass of the two electrodes, and *I* is the current. A specific capacitance of 72 F g^{-1} was delivered at 1 A g^{-1}, reducing with increasing current density to 36 F g^{-1} at 8 A g^{-1}.

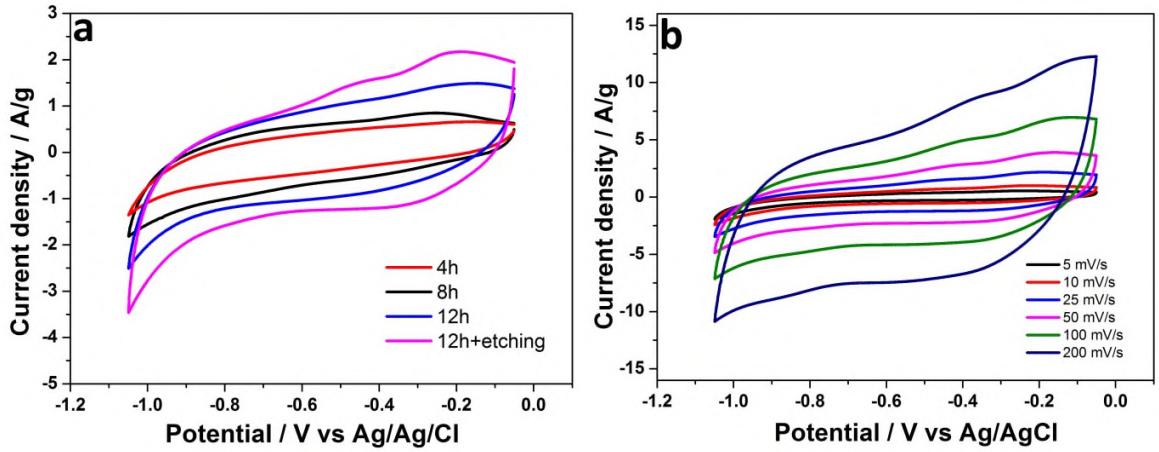

Figure 4 (a) CV curves of the mill scale ball milled at 4, 8, 12 hr and then HCl etched at a scan rate of 25 mV s^{-1}, and (b) CV curves of the HCl etched mill scale at various scan rates.

Table S1 gives the specific capacitances of iron oxide-based electrodes from the recent literature, indicating that the etched mill scale performance lies approximately in the mid-range of reported performance for similar scan rates. Note however that most of the data in Table S1 concerned small-scale laboratory synthesised iron oxides. In contrast, mill scale is a low value by-product or even industrial waste feedstock, abundantly available, processed here by facile industrial processes that already can operate at large scale. The implied lower cost, scalability and reasonable capacitance of mill scale, combined with a cheap aqueous electrolyte, suggest possible applications in grid scale energy storage, where very large electrode areas and large amounts of cheap electrode materials will be required.

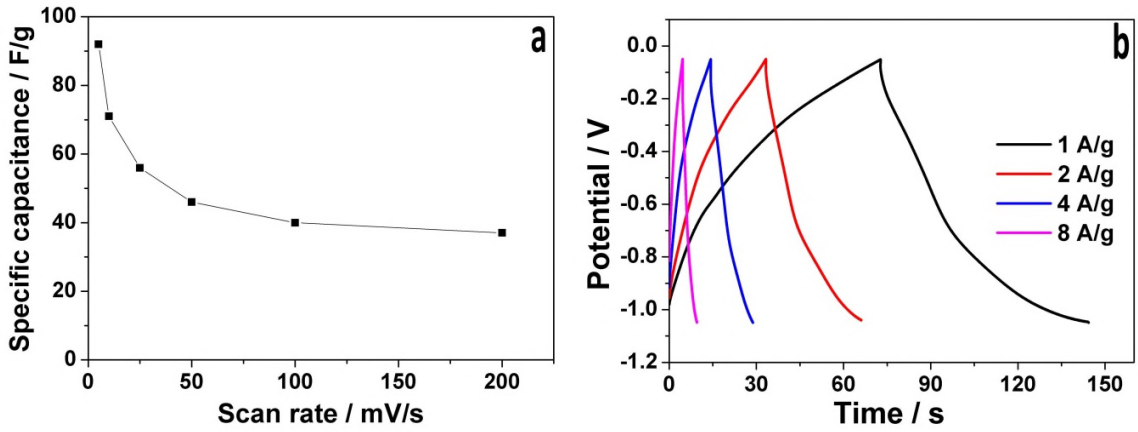

Figure 5 (a) Specific capacitance as a function of scan rate, and (b) galvanostatic discharge curves at various current densities, each for 12 hr ball milled mill scale followed by HCl etching.

The cycling performance of a FeO_x electrode in a three-electrode system is shown in Fig. 6a, with a slight increase in capacitance of ~3% over the first few cycles (possibly due to the relative instability of $Fe_{0.942}O$), which resulted from irreversible conversion of some of the mixed oxide phases. Beyond, this region, 83% capacitance was retained over 5,000 cycles. EIS was also conducted at open circuit potential, and Fig. 6b shows Nyquist plots of FeO_x in Na_2SO_3 before and after cycling. The Nyquist plots were best-fitted to the Randles-type equivalent circuit illustrated in Fig. 6c. The double-layer capacitance and the Warburg impedance were represented by two constant phase elements CPE_1 and CPE_2. Fitting of the equivalent circuit was carried out using Gamry Electrochemical Analyst software, and the parameters extracted. In the high frequency region, the intercept on the Z_{real} x-axis was almost the same both before cycling and after 5,000 cycles at 4.8 ± 0.1 Ω, indicating a moderate equivalent series resistance. The best-fit diameter of the semi-circle can be interpreted as the charge transfer resistance (R_{ct}) associated with Faradic redox reactions, and showed a small increase from 3.2 ± 0.1 to 10.9 ±

0.1 Ω after 5,000 cycles. The small resistance increase was mainly due to the slight electrode material expansion during repeated redox reactions. However, the SEM images of the FeO_x electrodes before and after long term cycling in Fig. S4 displayed no obvious change, suggesting good morphological stability at the macro-scale.

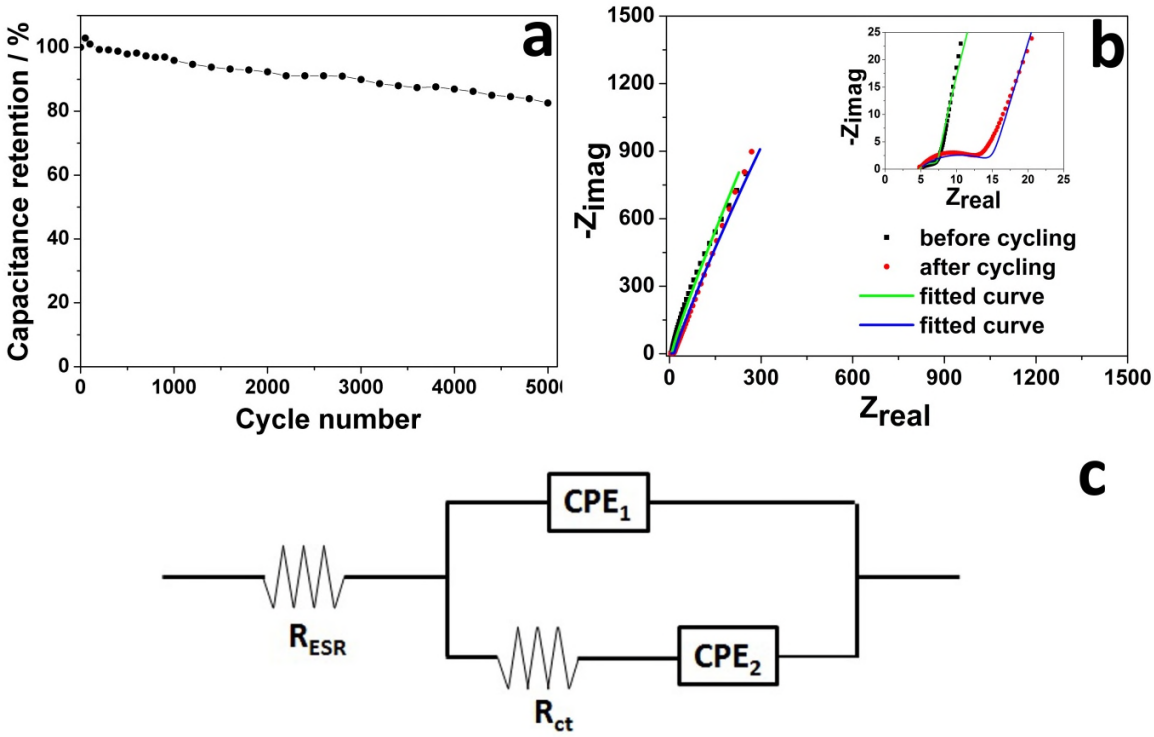

Figure 6 (a) Cycling performance of the FeO_x electrode, (b) experimental and fitted Nyquist plots of the FeO_x electrode in a Na_2SO_3 electrolyte, and (c) the equivalent circuit used to fit the data.

An aqueous based Na_2SO_3 electrolyte symmetric full cell supercapacitor coin cell was constructed and CV behaviour investigated in the range 0 to 1 V at scan rates from 5 to 100 mV s^{-1}. Fig. 7a shows that the CV curves at all scan rates showed a quasi-rectangular, distorted shape, indicative of some resistive character, as is commonly found in pseudo-capacitor full

cells. The specific capacitance was estimated using Equation (4) at 20 F g^{-1} at a scan rate of 5 mV s^{-1}. The charge/discharge behaviour at different current densities was also investigated in Fig. 7b, and similarly to half-cell data, again deviated from linear and were typical of pseudo-capacitors.[5, 20] The specific capacitance was estimated using Equation (5) at 25 F g^{-1} at a current density of 0.25 A g^{-1}, equivalent to a specific capacitance of 100 F g^{-1} for a single FeO_x electrode, and consistent with the earlier half cell data.

A Ragone plot using data from the full cell arrangement is shown in Fig. 8, which also contains comparative recent aqueous-based supercapacitor data re-plotted from the literature, indicating that the mill scale energy and power performance was broadly comparable to other aqueous-based symmetric supercapacitor systems, including the most comparable MnO_2 based arrangements.[37-40]

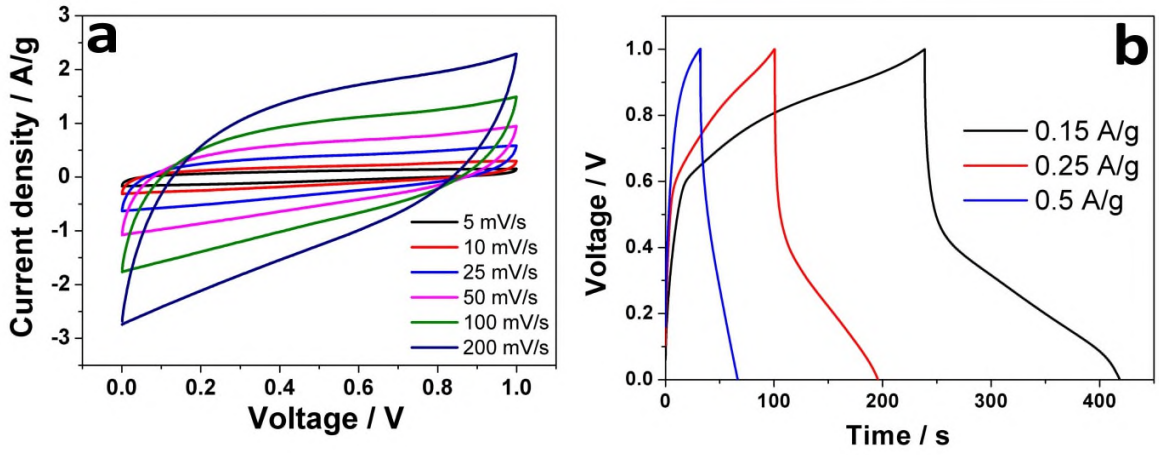

Figure 7 (a) CV curves of a full cell supercapacitor based on FeO_x at various scan rates, (b) galvanostatic charge/discharge curves of the same full cell supercapacitor at various current densities.

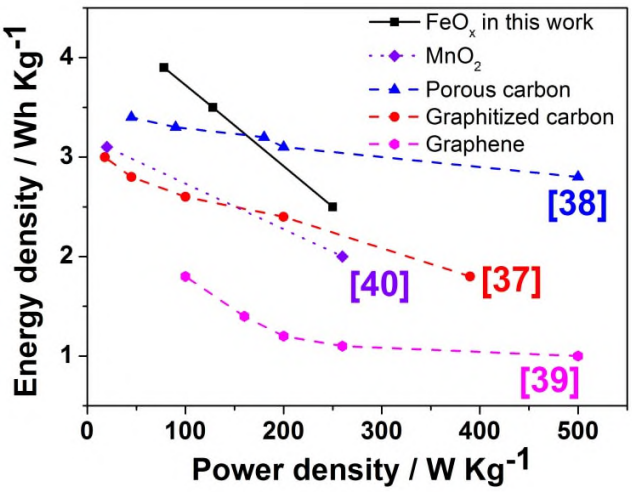

Figure 8 A Ragone plot constructed from data in Figure 7b, together with some comparative re-plotted data of aqueous-based symmetric supercapacitors.

Cost implications

A preliminary assessment of the implications of using mill scale based electrodes was undertaken. Assuming the mill scale chunks are essentially without cost, the processing costs are electricity consumed, the acid treatment, and associated equipment usage. The total cost of mill scale electrodes was estimated, as shown in Table S2, at ~23 USD kg^{-1}, based on the laboratory scale production of ~100 g described earlier. It is not unreasonable to assume that these costs could be reduced if the same approach were pursued at large scale. A "capacitance cost" was then estimated and compared with electrodes made from ~100 g of commercially available Fe_3O_4 nano-powders (Sigma, UK) and activated carbon (YP-50 AC, Kuraray Chemical Co., Ltd.) as described below. Fe_3O_4 was chosen because it was the largest fraction phase in the mill scale, and AC was chosen because it is the main electrode material used in commercial supercapacitors. It is recognised that the cost of commercial materials could be substantially

lower if purchased in bulk, but in the absence of any alternative robust and citable cost data, the actual costs incurred in our experiments were used in the cost comparison. In any case, as shown later, the low cost of mill scale will likely dominate its overall attractive cost weighted performance.

In order to obtain an estimate of the capacitance costs, electrodes were fabricated identically from FeO_x, commercial Fe_3O_4 and AC followed by identical CV testing in the same Na_2SO_3 electrolyte, so that non-feedstock costs could be assumed constant (the performance of the commercial materials in more typical electrolytes is investigated later). Fig. 9a shows the resulting CV curves with rather similar mass normalised current density responses. Table S3 shows the estimated specific capacitance from these data and the capacitance cost was then estimated from:

$$\text{Capacitance cost (USD/F)} = \frac{\text{Unit price (USD/g)}}{\text{Specific capacitance (F/g)}} \qquad (5)$$

The estimated capacitance costs are shown in Fig. 9b, with the relatively restricted absolute gravimetric capacitance of mill scale more strongly compensated for by its negligible feedstock cost: unrealistically high cost would have to be ascribed to the feedstock mill scale, or *very* large discounts applied to the commercial materials, to give mill scale a similar capacitance cost in this configuration.

The energy cost (USD/kWh) and power cost (USD/kW) for the mill scale supercapacitors were also estimated, assuming that the electrode materials accounted for 65% of the total capacitance cost (since comparatively cheap aqueous-based electrolytes were employed and not more expensive organic electrolytes), and ignoring in-service costs:

$$\text{Energy cost (USD/kWh)} = \frac{\text{Unit price (USD/Kg)}}{65\% * \text{Energy density (kWh/kg)}} \quad (6)$$

$$\text{Power cost (USD/kW)} = \frac{\text{Unit price (USD/Kg)}}{65\% * \text{Power density (kW/kg)}} \quad (7)$$

The corresponding energy and power costs, as well as similar data for commercial LIBs and carbon/carbon based supercapacitors in their bespoke electrolytes used commercially are shown in Fig. 10, using LIB and supercapacitor data aggregated from various sources.[41-44] As is well known, Fig. 10 shows that supercapacitors are characterized by high energy cost while LIBs are characterized by high power cost. However, the energy and power costs of the mill scale supercapacitors, using our laboratory data, are nonetheless broadly competitive with commercial devices. It should be noted that the aqueous-based mill scale supercapacitor has a working voltage of only 1 V, compared with up to ~3 V for commercial LIBs and supercapacitors. Since energy density is proportional to the square of working voltage, small increases, for example by the use of asymmetric electrode arrangements, such as mill scale versus cheap bio-derived carbon, could significantly increase the relative attractiveness of the mill scale.[40] Of course, these cost estimations and comparisons are, at best, only first order and somewhat crude. However, the literature provides little data or help on how to construct a more robust cost-benefit analysis of even this relatively coarse type. A common approach to a first order quantification of the forecast cost-benefit for new energy storage materials or systems would be extremely useful for researchers to understand better their potential restrictions and opportunities.

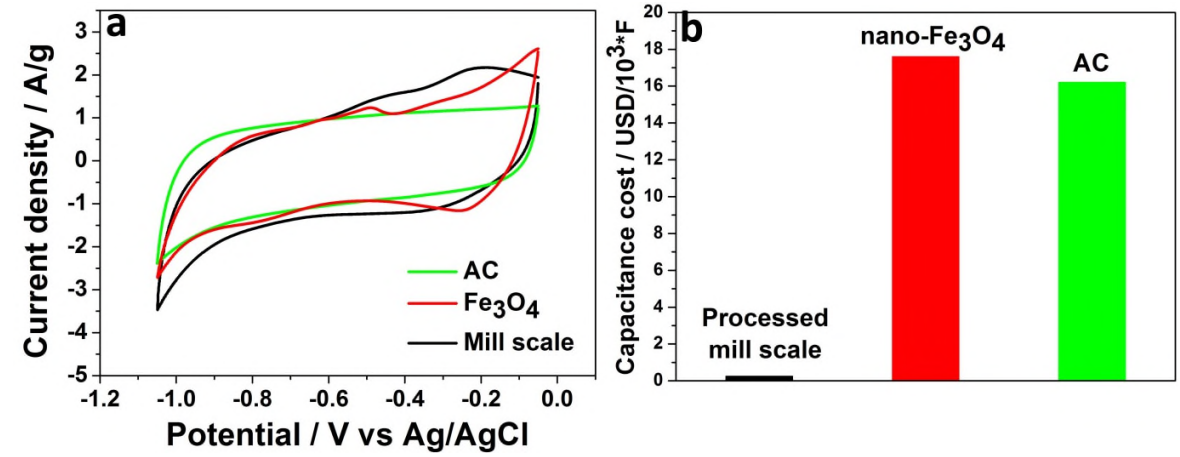

Figure 9 (a) CV curves of the processed mill scale (FeO_x), commercial Fe_3O_4 nanoparticles and activated carbon (AC) electrodes in the same Na_2SO_3 electrolyte and produced in the same way; and (b) approximate capacitance cost for the same electrode materials.

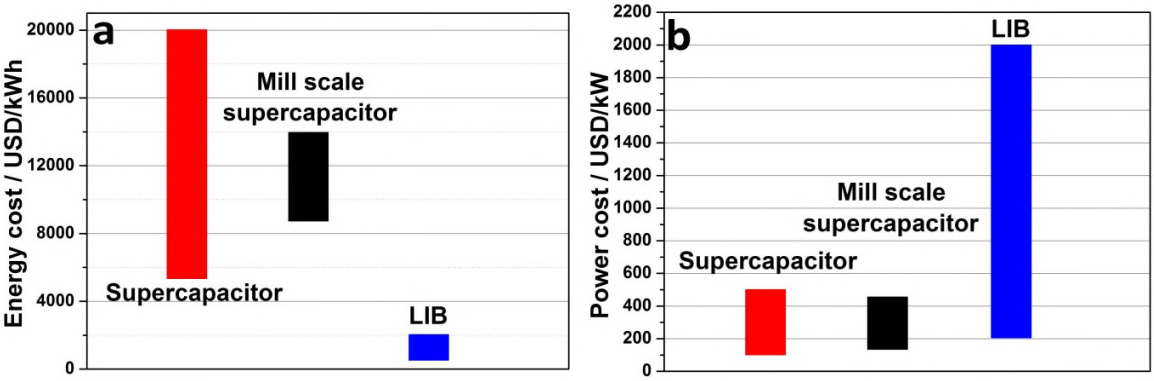

Figure 10 (a) Energy and (b) power cost estimations for mill scale supercapacitors, and commercial LIBs and supercapacitors.

Conclusions

Supercapacitor electrodes based on industrial waste mill scale have been prepared from suspension by spray deposition. The as-supplied mill scale was firstly milled to approximately 1 µm particles and then treated in hydrochloric acid. The resulting powder comprised Fe_2O_3,

Fe_3O_4 and $Fe_{0.942}O$, and a small fraction of metallic iron, with a BET surface area of 9.5 m^2 g^{-1}. Electrochemical testing showed a capacitance of 92 F g^{-1} at 5 mV s^{-1} in a half cell arrangement and 25 F g^{-1} at 0.25 A g^{-1} in a full cell arrangement in an aqueous Na_2SO_3 electrolyte. Capacitance was retained at 83% of its initial value after 5,000 cycles. The cost of devices fabricated from mill scale was assessed approximately, compared with commercial counterparts and showed promising potential for large scale energy storage applications while the need for better models for cost-benefit cross-comparisons was emphasised. More generally it was shown that ideas already advanced to exploit low cost, abundant materials and simple processing for electric double layer capacitor electrodes might also usefully be applied in some cases for pseudo-capacitive materials.

Acknowledgement

The authors would like to thank the UK Engineering and Physical Sciences Research Council (Grant EP/K002252/1) for financial support, Tata Steel Long Product Rolling, UK for kindly supplying the mill scale, and Dr Phil Holdway for help with XRD analysis.

References

1. Han, S.; Wu, D.; Li, S.; Zhang, F.; Feng, X. Porous Graphene Materials for Advanced Electrochemical Energy Storage and Conversion Devices. *Adv. Mater.* 2014, 26, 849-864.

2. Wang, G.; Zhang, L.; Zhang, J. A review of electrode materials for electrochemical supercapacitors. *Chem. Soc. Rev.* 2012, 41, 797-828.

3. Fu, C.; Zhou, H.; Liu, R.; Huang, Z.; Chen, J.; Kuang, Y. Supercapacitor based on electropolymerized polythiophene and multi-walled carbon nanotubes composites. *Mater. Chem. Phys.* 2012, 132, 596-600.

4. Jiang, H.; Li, C.; Sun, T.; Ma, J. High-performance supercapacitor material based on $Ni(OH)_2$ nanowire-MnO_2 nanoflakes core-shell nanostructures. *Chem. Commun.* 2012, 48, 2606-2608.

5. Yuan, C.; Li, J.; Hou, L.; Zhang, X.; Shen, L.; Lou, X. W. Ultrathin Mesoporous $NiCo_2O_4$ Nanosheets Supported on Ni Foam as Advanced Electrodes for Supercapacitors. *Adv. Funct. Mater.* 2012, 22, 4592-4597.

6. Lu, Q.; Lattanzi, M. W.; Chen, Y.; Kou, X.; Li, W.; Fan, X.; Unruh, K. M.; Chen, J. G.; Xiao, J. Q. Supercapacitor Electrodes with High-Energy and Power Densities Prepared from Monolithic NiO/Ni Nanocomposites. *Angew. Chem. Int. Ed.* 2011, 50, 6847-6850.

7. Lien, C. H.; Hu, C. C.; Hsu, C. T.; Wong, D. S. H. High-performance asymmetric supercapacitor consisting of Ni-Co-Cu oxy-hydroxide nanosheets and activated carbon. *Electrochem. Commun.* 2013, 34, 323-326.

8. Tian, W.; Wang, X.; Zhi, C. Y.; Zhai, T. Y.; Liu, D. Q.; Zhang, C.; Golberg, D.; Bando, Y. $Ni(OH)_2$ nanosheet@Fe2O3 nanowire hybrid composite arrays for high-performance supercapacitor electrodes. *Nano Energy* 2013, 2, 754-763.

9. Liu, T. C.; Pell, W. G.; Conway, B. E. Self-discharge and potential recovery phenomena at thermally and electrochemically prepared RuO_2 supercapacitor electrodes. *Electrochim. Acta* 1997, 42, 3541-3552.

10. Wu, X.; Zeng, Y.; Gao, H. R.; Su, J.; Liu, J. P.; Zhu, Z. H. Template synthesis of hollow fusiform RuO_2•xH_2O nanostructure and its supercapacitor performance. *J. Mater. Chem. A* 2013, 1, 469-472.

11. Ye, C.; Lin, Z. M.; Hui, S. Z. Electrochemical and capacitance properties of rod-shaped MnO_2 for supercapacitor. *J. Electrochem. Soc.* 2005, 152, A1272-A1278.

12. Chen, Q.; Meng, Y. N.; Hu, C. G.; Zhao, Y.; Shao, H. B.; Chen, N.; Qu, L. T. MnO_2-modified hierarchical graphene fiber electrochemical supercapacitor. *J. Power Sources* 2014, 247, 32-39.

13. Yu, Z. N.; Duong, B.; Abbitt, D.; Thomas, J. Highly Ordered MnO_2 Nanopillars for Enhanced Supercapacitor Performance. *Adv. Mater.* 2013, 25, 3302-3306.

14. Jiang, H.; Yang, L. P.; Li, C. Z.; Yan, C. Y.; Lee, P. S.; Ma, J. High-rate electrochemical capacitors from highly graphitic carbon-tipped manganese oxide/mesoporous carbon/manganese oxide hybrid nanowires. *Energy. Environ. Sci.* 2011, 4, 1813-1819.

15. Jagadale, A. D.; Kumbhar, V. S.; Dhawale, D. S.; Lokhande, C. D. Performance evaluation of symmetric supercapacitor based on cobalt hydroxide $Co(OH)_2$ thin film electrodes. *Electrochim. Acta* 2013, 98, 32-38.

16. Lee, G. H.; Cheng, Y. W.; Varanasi, C. V.; Liu, J. Influence of the Nickel Oxide Nanostructure Morphology on the Effectiveness of Reduced Graphene Oxide Coating in Supercapacitor Electrodes. *J. Phys. Chem. C* 2014, 118, 2281-2286.

17. Wang, X.; Yan, C. Y.; Sumboja, A.; Lee, P. S. High performance porous nickel cobalt oxide nanowires for asymmetric supercapacitor. *Nano Energy* 2014, 3, 119-126.

18. Zhang, J.; Wang, X. C.; Ma, J.; Liu, S.; Yi, X. B. Preparation of cobalt hydroxide nanosheets on carbon nanotubes/carbon paper conductive substrate for supercapacitor application. *Electrochim. Acta* 2013, 104, 110-116.

19. Binitha, G.; Soumya, M. S.; Madhavan, A. A.; Praveen, P.; Balakrishnan, A.; Subramanian, K. R. V.; Reddy, M. V.; Nair, S. V.; Nair, A. S.; Sivakumar, N. Electrospun alpha-Fe_2O_3 nanostructures for supercapacitor applications. *J. Mater. Chem. A* 2013, 1, 11698-11704.

20. Lee, K. K.; Deng, S.; Fan, H. M.; Mhaisalkar, S.; Tan, H. R.; Tok, E. S.; Loh, K. P.; Chin, W. S.; Sow, C. H. alpha-Fe_2O_3 nanotubes-reduced graphene oxide composites as synergistic electrochemical capacitor materials. *Nanoscale* 2012, 4, 2958-2961.

21. Liu, J.; Liu, S. Q.; Zhuang, S. X.; Wang, X. W.; Tu, F. Y. Synthesis of carbon-coated Fe_3O_4 nanorods as electrode material for supercapacitor. *Ionics* 2013, 19, 1255-1261.

22. Shivakumara, S.; Penki, T. R.; Munichandraiah, N. Synthesis and Characterization of Porous Flowerlike alpha-Fe_2O_3 Nanostructures for Supercapacitor Application. *ECS Electrochem. Lett.* 2013, 2, A60-A62.

23. Wang, L.; Ji, H. M.; Wang, S. S.; Kong, L. J.; Jiang, X. F.; Yang, G. Preparation of Fe_3O_4 with high specific surface area and improved capacitance as a supercapacitor. *Nanoscale* 2013, 5, 3793-3799.

24. O'Neill, L.; Johnston, C.; Grant, P. S. Enhancing the supercapacitor behaviour of novel Fe_3O_4/FeOOH nanowire hybrid electrodes in aqueous electrolytes. *J. Power Sources* 2015, 274, 907-915.

25. Zhao, X.; Johnston, C.; Crossley, A.; Grant, P. S. Printable magnetite and pyrrole treated magnetite based electrodes for supercapacitors. *J. Mater. Chem.* 2010, 20, 7637-7644.

26. Lv, Y.; Gan, L.; Liu, M.; Xiong, W.; Xu, Z.; Zhu, D.; Wright, D. S. A self-template synthesis of hierarchical porous carbon foams based on banana peel for supercapacitor electrodes. *J. Power Sources* 2012, 209, 152-157.

27. Galinski, M.; Babeł, K.; Jurewicz, K. Performance of an Electrochemical double layer capacitor based on coconut shell active material and ionic liquid as an electrolyte. *J. Power Sources* 2013, 228, 83-88.

28. Lee, M.; Kim, G. P.; Song, H. D.; Park, S.; Yi, J. Preparation of energy storage material derived from a used cigarette filter for a supercapacitor electrode. *Nanotechnology* 2014, 25, 345601-345608.

29. Zhao, X.; Hinchliffe, C.; Johnston, C.; Dobson, P. J.; Grant, P. S. Spray deposition of polymer nanocomposite films for dielectric applications. *Mater. Sci. Eng. B* 2008, 151, 140-145.

30. Chung, F. H. Quantitative interpretation of X-ray diffraction patterns of mixtures. II. Adiabatic principle of X-ray diffraction analysis of mixtures. *J. Appl. Crystallogr.* 1974, 7, 526-531.

31. Chung, F. Quantitative interpretation of X-ray diffraction patterns of mixtures. I. Matrix-flushing method for quantitative multicomponent analysis. *J. Appl. Crystallogr.* 1974, 7, 519-525.

32. Shoemaker, R. S.; Harris, D. L. QUANTITATIVE USE OF X-RAY DIFFRACTION FOR ANALYSIS OF IRON OXIDES IN GOGEBIC TACONITE OF WISCONSIN. *Transactions of the American Institute of Mining and Metallurgical Engineers* 1955, 202, 476-480.

33. Hubbard, C. R.; Evans, E. H.; Smith, D. K. The reference intensity ratio, I/Ic, for computer simulated powder patterns. *J. Appl. Crystallogr.* 1976, 9, 169-174.

34. Wang, S. Y.; Ho, K. C.; Kuo, S. L.; Wu, N. L. Investigation on capacitance mechanisms of Fe3O4 electrochemical capacitors. *J. Electrochem. Soc.* 2006, 153, A75-A80.

35. Long, C.; Wei, T.; Yan, J.; Jiang, L.; Fan, Z. Supercapacitors Based on Graphene-Supported Iron Nanosheets as Negative Electrode Materials. *ACS Nano* 2013, 7, 11325-11332.

36. Li, Z.; Xu, Z.; Wang, H.; Ding, J.; Zahiri, B.; Holt, C. M. B.; Tan, X.; Mitlin, D. Colossal pseudocapacitance in a high functionality-high surface area carbon anode doubles the energy of an asymmetric supercapacitor. *Energy. Environ. Sci.* 2014, 7, 1708-1718.

37. Mun, Y.; Jo, C.; Hyeon, T.; Lee, J.; Ha, K. S.; Jun, K. W.; Lee, S. H.; Hong, S. W.; Lee, H. I.; Yoon, S.; Lee, J. Simple synthesis of hierarchically structured partially graphitized carbon by emulsion/block-copolymer co-template method for high power supercapacitors. *Carbon* 2013, 64, 391-402.

38. He, X.; Zhao, N.; Qiu, J.; Xiao, N.; Yu, M.; Yu, C.; Zhang, X.; Zheng, M. Synthesis of hierarchical porous carbons for supercapacitors from coal tar pitch with nano-Fe_2O_3 as template and activation agent coupled with KOH activation. *J. Mater. Chem. A* 2013, 1, 9440-9448.

39. Wu, Z. S.; Ren, W.; Wang, D.-W.; Li, F.; Liu, B.; Cheng, H. M. High-Energy MnO_2 Nanowire/Graphene and Graphene Asymmetric Electrochemical Capacitors. *ACS Nano* 2010, 4, 5835-5842.

40. Long, J. W.; Belanger, D.; Brousse, T.; Sugimoto, W.; Sassin, M. B.; Crosnier, O. Asymmetric electrochemical capacitors-Stretching the limits of aqueous electrolytes. *MRS Bull.* 2011, 36, 513-522.

41. Miller J. R.; Burke A. F. Electrochemical capacitors: Challenges and opportunities for real-world applications. *Electrochem. Soc. Interface*, 2008, 17, 53-57.

42. SBC Energy Institute, Electricity Storage, online available:

http://www.sbc.slb.com/SBCInstitute/Publications/ElectricityStorage.aspx

43. Supercapacitor, Factsheet to accompany the report “Pathways for energy storage in the UK”, online available:

http://www.lowcarbonfutures.org/sites/default/files/supercapacitator.pdf

44. Battery university, supercapacitor, online available:

http://batteryuniversity.com/learn/article/whats_the_role_of_the_supercapacitor

For Table of Contents Use Only

Towards low cost grid scale energy storage: supercapacitors based on up-cycled industrial mill scale waste

Chaopeng Fu, Patrick S. Grant

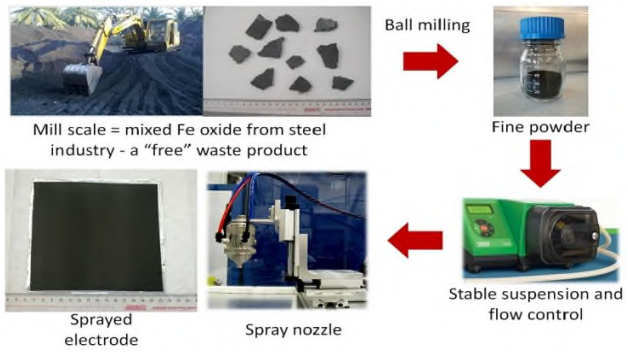

An industrial waste mill scale has successfully been up-cycled into a high-added value material for energy storage.

Supporting Information

Towards low cost grid scale energy storage: supercapacitors based on up-cycled industrial mill scale waste

Chaopeng Fu,* Patrick S. Grant

Department of Materials, University of Oxford, Oxford, United Kingdom, OX1 3PH.

* E-mail: chaopeng.fu@materials.ox.ac.uk

Number of pages: 6

Number of figures: 4

Number of tables: 3

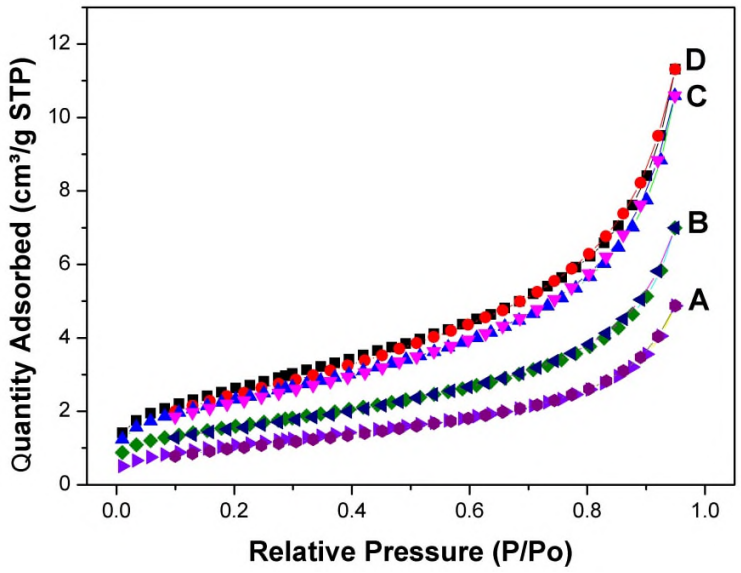

Figure S1 N_2 adsorption-desorption isotherms of the mill scale processed by ball milling for (A) 4 hr, (B) 8 hr, (C) 12 hr, and (D) 12 hr followed by chemical etching.

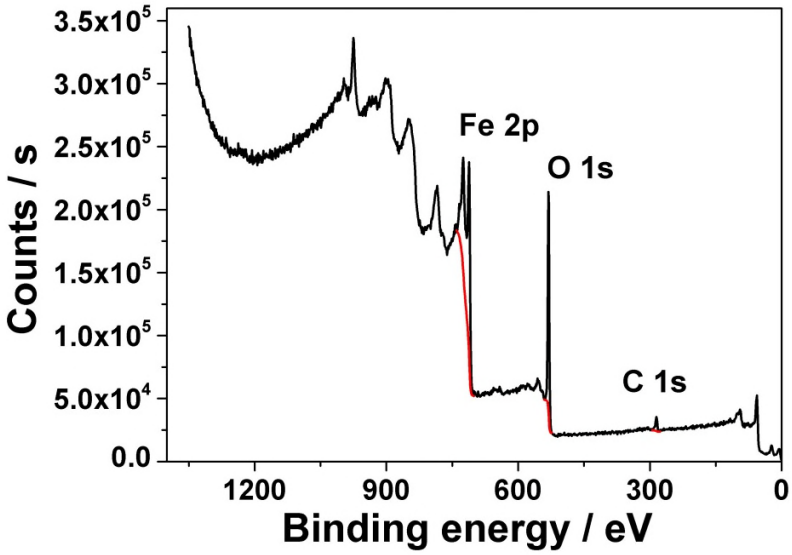

Figure S2 XPS suvey scan of the mill scale powder. The detected carbon was from the air.

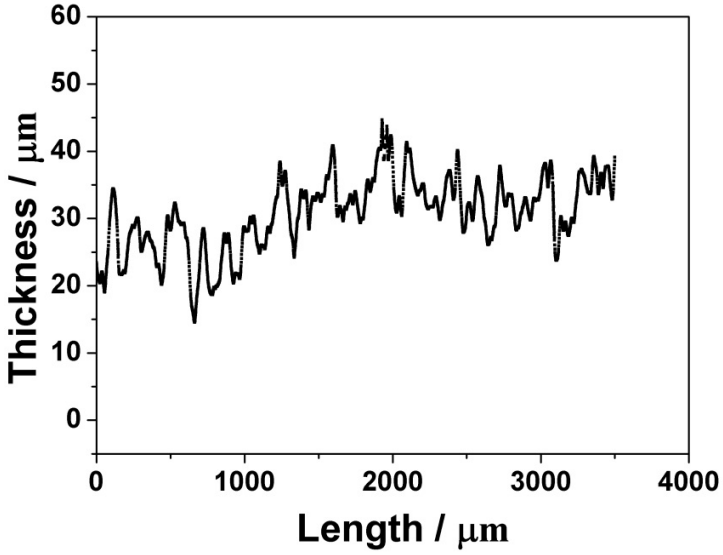

Figure S3 Thickness profile across a 3.5 μm portion of the as-sprayed mill scale electrode.

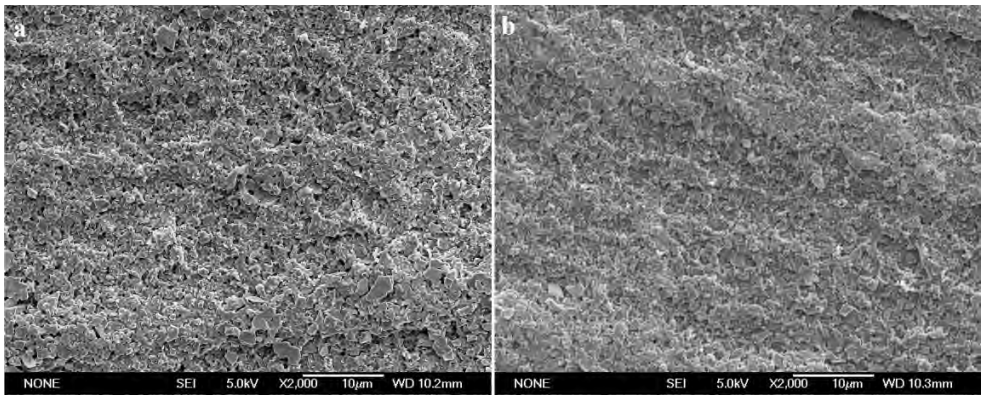

Figure S4 SEM images of the mill scale electrode (a) before and (b) after cycling.

Table S1 The specific capacitances of iron oxides reported in recent publications.

Material	Electrolyte	Current density or scan rate	Capacitance F/g	Reference
Fe_2O_3	Na_2SO_4	10 mV/s	90	[1]
Fe_3O_4 nanosheets/CNF	Na_2SO_3	10 mV/s	127	[2]
Fe_3O_4 nanowires	Na_2SO_3	1 A/g	60	[3]
Fe_3O_4 nanorods	Na_2SO_3	1 A/g	30	[3]
Fe_2O_3 porous fiber	LiOH	1 mV/s	256	[4]
Fe_2O_3 nanograin	LiOH	1 mV/s	102	[4]
Fe_3O_4 nanoparticles	KOH	5 mV/s	58	[5]
Fe_2O_3	Na_2SO_4	20 mV/s	23	[6]
Fe_2O_3/graphene	Na_2SO_4	2.5 mV/s	113	[6]
Fe_2O_3	Na_2SO_3	1 A/g	127	[7]
Fe_2O_3 sheets	Li_2SO_4	0.36 A/g	147	[8]

Table S2 Cost estimation of the processed mill scale.

Mill scale cost /batch=160 g[a]	USD
Electricity	3.0[b]
Acid treatment	0.4
Ball mill machine/pot usage	0.2
Other	0.1
Sum	3.7
Total cost	23.1 USD/kg

[a] Four balls were used in each ball milling container, and 40 g of powder were obtained from each pot.

[b] The ball milling consumed electricity of 14.4 kWh, at a local electricity unit price of 0.13 GBP/kWh (1 GBP=1.6 USD).

Table S3 Specific capacitance and capacitance cost for mill scale, commerical Fe_3O_4 nano-powder and commercial activated carbon (AC)

Materials	Specific capacitance F g^{-1} @5 mV/s	Capacitance cost (USD/10^3F)	Cost (USD/kg)	Source
Processed mill scale	92	0.25	23.1 (USD3.7/160 g)	Steel plant (UK) + in-house processing
Nano-Fe_3O_4	79	17.6	1,391 (USD139/100 g)	Sigma-Aldrich (UK), product code: 637106
Activated carbon YP-50	72	16.2	1,167 (USD350/300 g)	Kuraray Chemical Co. (Japan)

Reference

1. M. S. Wu, R. H. Lee, J. J. Jow, W. D. Yang, C. Y. Hsieh and B. J. Weng, *Electrochemical and Solid State Letters*, 2009, 12, A1-A4.
2. J. B. Mu, B. Chen, Z. C. Guo, M. Y. Zhang, Z. Y. Zhang, P. Zhang, C. L. Shao and Y. C. Liu, *Nanoscale*, 2011, 3, 5034-5040.
3. X. Zhao, C. Johnston, A. Crossley and P. S. Grant, *Journal of Materials Chemistry*, 2010, 20, 7637-7644.
4. G. Binitha, M. S. Soumya, A. A. Madhavan, P. Praveen, A. Balakrishnan, K. R. V. Subramanian, M. V. Reddy, S. V. Nair, A. S. Nair and N. Sivakumar, *Journal of Materials Chemistry A*, 2013, 1, 11698-11704.
5. X. Du, C. Wang, M. Chen, Y. Jiao and J. Wang, *The Journal of Physical Chemistry C*, 2009, 113, 2643-2646.
6. K. K. Lee, S. Deng, H. M. Fan, S. Mhaisalkar, H. R. Tan, E. S. Tok, K. P. Loh, W. S. Chin and C. H. Sow, *Nanoscale*, 2012, 4, 2958-2961.
7. S. Shivakumara, T. R. Penki and N. Munichandraiah, *ECS Electrochemistry Letters*, 2013, 2, A60-A62.
8. J. C. Huang, S. N. Yang, Y. Xu, X. B. Zhou, X. Jiang, N. N. Shi, D. X. Cao, J. L. Yin and G. L. Wang, *J. Electroanal. Chem.*, 2014, 713, 98-102.